J|A|C|S
ARTICLES

Published on Web 11/01/2010

High-Pressure Synthesis and Local Structure of Corundum-Type $In_{2-2x}Zn_xSn_xO_3$ ($x \leq 0.7$)

Cathleen A. Hoel,[†] José Manuel Gallardo Amores,[‡] Emilio Morán,[‡] Miguel Angel Álario-Franco,[‡] Jean-François Gaillard,[§] and Kenneth R. Poeppelmeier*,[†]

Department of Chemistry and Department of Civil and Environmental Engineering, Northwestern University, 2145 Sheridan Road, Evanston, Illinois 60208, United States, and Departamento de Química Inorgánica I, Universidad Complutense, 28040 Madrid, Spain

Received July 8, 2010; E-mail: krp@northwestern.edu

Abstract: The corundum-type $In_{2-2x}Zn_xSn_xO_3$ solid solution (*cor*-ZITO, $x \leq 0.7$) was synthesized at 1000 °C under a high pressure of 70 kbar. *cor*-ZITO is a high-pressure polymorph of the transparent conducting oxide bixbyite-$In_{2-2x}Zn_xSn_xO_3$ ($x \leq 0.4$). Analysis of the extended X-ray absorption fine structure suggests that significant face-sharing of Zn and Sn octahedra occurs, as expected for the corundum structure type. In contrast to the ideal corundum structure, however, Zn and Sn are displaced and form oxygen bonds with lengths that are similar to those observed in high-pressure $ZnSnO_3$. Powder X-ray diffraction patterns of *cor*-ZITO showed the expected unit cell contraction with increased cosubstitution, but no evidence for ilmenite-type ordering of the substituted Zn and Sn. A qualitative second harmonic generation measurement, for the solid solution $x = 0.6$ and using 1064 nm radiation, showed that Zn and Sn adopt a polar $LiNbO_3$-type arrangement.

Introduction

Photovoltaic devices, flat-panel displays, and optoelectronics require a transparent conducting oxide (TCO) layer to pass electrical current through the device and to transmit the visible light absorbed/emitted by the active layer.[1,2] The most common TCO anode for high-end electronics is Sn-doped In_2O_3 (ITO) with conductivities ranging from 10^3 to 10^4 S/cm and over 90% visible transparency in thin film form.[3,4] The scarcity and high cost of indium metal has driven the TCO market to develop less expensive alternatives, such as $In_{2-2x}Zn_xSn_xO_3$ ($x \leq 0.4$, or ZITO).[5−7] ZITO exhibits up to 40% indium substitution (cation basis) and has proven to be competitive with ITO with conductivities reaching 5000 S/cm and over 85% visible transparency.[5−7] This work reports the synthesis of the corundum polymorph of ZITO (*cor*-ZITO), which exhibited up to 70% indium substitution. The preferable TCO would contain no indium and likely belong to the Zn−Sn−O (ZTO) system.[7]

In_2O_3 and ZITO adopt the bixbyite structure type at ambient pressures.[5,8,9] Bixbyite In_2O_3 (*bix*-In_2O_3) transitions to the corundum structure (*cor*-In_2O_3) at 65 kbar and 1000 °C, which can be quenched to a metastable state at ambient pressures.[10,11] Single crystals of *cor*-In_2O_3, grown from a NaOH flux,[12] had conductivities on the order of 10^3 S/cm, and Sn-doped crystals (~2% Sn) exhibited conductivities of 10^4 S/cm.[11] In 2008, Inaguma et al.[13] reported the synthesis of $ZnSnO_3$ by a solid-state reaction at 70 kbar and 1000 °C. $ZnSnO_3$ was found to adopt the $LiNbO_3$ structure type (*LN*-$ZnSnO_3$), a daughter structure of corundum. The isotypic relationship between *cor*-In_2O_3 and *LN*-$ZnSnO_3$ was expected to facilitate the formation of the corundum-type $In_{2-2x}Zn_xSn_xO_3$ solid solution at high pressures. This paper reports an extensive structural study of the *cor*-ZITO solid solution that probes the long-range cation ordering with high-resolution X-ray diffraction (HR-XRD) and the local structure of each cation with a multishell analysis of the extended X-ray absorption fine structure (EXAFS).

Cation Ordering of $ZnSnO_3$ ($x = 1.0$). Cation ordering in multicomponent systems will influence the material's properties, so further discussion on this topic is warranted to fully characterize the *cor*-$In_{2-2x}Zn_xSn_xO_3$ solid solution. The corundum (α-Al_2O_3) structure can be described as hexagonal closed-packed anions with cations filling two-thirds of the octahedral

[†] Department of Chemistry, Northwestern University.
[‡] Universidad Complutense.
[§] Department of Civil and Environmental Engineering, Northwestern University.

(1) Edwards, P. P.; Porch, A.; Jones, M. O.; Morgan, D. V.; Perks, R. M. *Dalton Trans.* **2004**, 2995–3002.
(2) Fortunato, E.; Ginley, D.; Hosono, H.; Paine, D. C. *MRS Bull.* **2007**, *32*, 242–247.
(3) Frank, G.; Kauer, E.; Kostlin, H. *Thin Solid Films* **1981**, *77*, 107–117.
(4) Rauf, I. A. *Mater. Lett.* **1993**, *18*, 123–127.
(5) Palmer, G. B.; Poeppelmeier, K. R.; Mason, T. O. *Chem. Mater.* **1997**, *9*, 3121–3126.
(6) Harvey, S. P.; Mason, T. O.; Buchholz, D. B.; Change, R. P. H.; Korber, C.; Klein, A. *J. Am. Ceram. Soc.* **2008**, *91*, 467–472.
(7) Hoel, C. A.; Mason, T. O.; Gaillard, J.-F.; Poeppelmeier, K. R. *Chem. Mater.* **2010**, *22*, 3569–3579.
(8) Marezio, M. *Acta Crystallogr.* **1966**, *20*, 723–728.
(9) Harvey, S. P.; Poeppelmeier, K. R.; Mason, T. O. *J. Am. Ceram. Soc.* **2008**, *91*, 3683–3689.
(10) Shannon, R. D. *Solid State Commun.* **1966**, *4*, 629–630.
(11) Prewitt, C. T.; Shannon, R. D.; Rodgers, D. B.; Sleight, A. W. *Inorg. Chem.* **1969**, *8*, 1985–1993.
(12) Remeika, J. P.; Marezio, M. *Appl. Phys. Lett.* **1966**, *8*, 87–88.
(13) Inaguma, Y.; Yoshida, M.; Katsumata, T. *J. Am. Chem. Soc.* **2008**, *130*, 6704–6705.

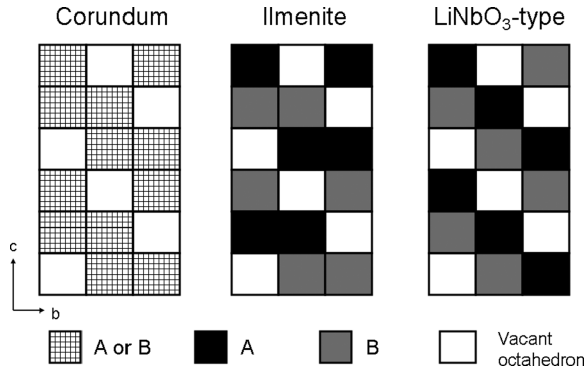

Figure 1. Illustration of three types of ordering in the parent corundum structure type. The face-sharing octahedra are aligned in the direction of the *c*-axis; i.e., the face-sharing plane is parallel to the *ab*-plane.

holes. Two cation octahedra are face-sharing such that the cations are in equivalent positions reflected across a mirror plane defined by the face-sharing oxygen. Corundum-type structures with an ABO_3 stoichiometry can exhibit long-range ordering of the two cations A and B. Three scenarios are illustrated in Figure 1.[14,15] The first scenario has A and B disordered, so that the corundum symmetry, $R\bar{3}c$, is maintained. The second scenario ($LiNbO_3$) has the face-sharing A−B units aligned in an additive manner along the *c*-axis, such that the inversion center is lost and the symmetry lowers to *R*3*c*. The third scenario (ilmenite) has the face-sharing A−B units aligned in alternating orientations so that the glide plane along the *c*-axis is lost and the symmetry lowers to $R\bar{3}$. The ilmenite-type ordering can be identified by powder XRD with the appearance of the (003) and (101) diffraction peaks, which are absent for the corundum and $LiNbO_3$ symmetry. Distinguishing the $LiNbO_3$ ordering from corundum ordering with powder diffraction is difficult because the space groups are restricted to the same reflection conditions.

$ZnSnO_3$ has been shown to form both the ilmenite-[16] and $LiNbO_3$-[13]type ordering depending on the synthesis route. Ilmenite-type $ZnSnO_3$ (*il*-$ZnSnO_3$) was synthesized by Li_2SnO_3 ion exchange with $ZnCl_2$.[16] *LN*-$ZnSnO_3$ was synthesized by high-pressure/high-temperature solid-state methods, which are the same synthesis conditions reported in this study for *cor*-ZITO.[13] *LN*-$ZnSnO_3$ was observed to be more dense than *il*-$ZnSnO_3$, which is consistent with the favored formation at high pressures.[13] Previous studies[17,18] of ABO_3 compounds reported an observed transition from ilmenite to disordered corundum at high pressures. Ko and Prewitt,[15] however, showed that $MnTiO_3$ transitioned from ilmenite to $LiNbO_3$ ordering at high pressures and suggested that other ilmenite oxides may also transition to $LiNbO_3$ ordering rather than the previously assumed disordered corundum.

An important distinction between *cor*-In_2O_3 and *LN*-$ZnSnO_3$ is the cation position in the octahedron. Corundum-In_2O_3 has units of two face-sharing octahedra such that two crystallographically equivalent In cations are reflected, or equidistant, across the face-sharing plane. The cations are displaced from the octahedral center by equal amounts and bond to 3 oxygen

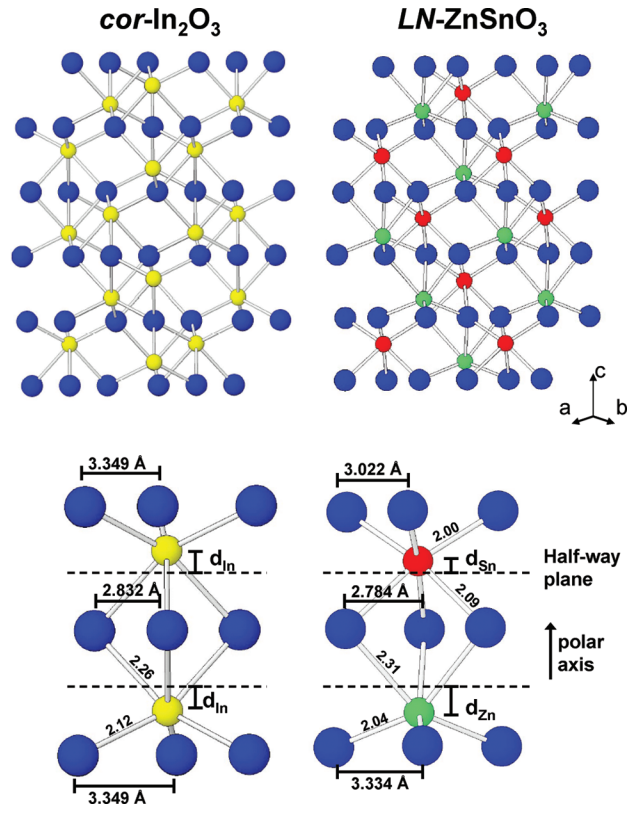

Figure 2. Corundum-type In_2O_3 and $LiNbO_3$-type $ZnSnO_3$ (top). Oxygen is blue, indium is yellow, tin is red, and zinc is green. Face-sharing octahedral units are isolated and enlarged (bottom). The plane that is halfway between the *c*-axis oxygen planes is marked with a dashed line. The face-sharing In cations in corundum are equivalent, but Zn and Sn in the *LN*-$ZnSnO_3$ structure reside at nonequivalent positions in the octahedra ($d_{Zn} > d_{Sn}$).

at 2.117 Å and 3 oxygen at 2.258 Å. The net effect is a cancellation of local dipoles, which yields a centrosymmetric extended structure. The *LN*-$ZnSnO_3$ structure, however, has ZnO_6 octahedra that share a face with SnO_6 octahedra, which creates a local dipole. These dipoles are oriented in the same direction such that the extended structure exhibits a polar moment along the *c*-axis.[19] A *LN*-$ZnSnO_3$ film experimentally demonstrated a ferroelectric response, which supported the $LiNbO_3$ cation ordering type.[13,20] The *LN*-$ZnSnO_3$ structure has the Sn and Zn displaced from the octahedron center by nonequivalent amounts. The ZnO_6 octahedra have 3 short bonds at 2.041 Å and 3 long bonds at 2.310 Å. The SnO_6 octahedron has 3 short bonds of 2.003 Å and 3 long bonds of 2.094 Å. The *cor*-In_2O_3 and *LN*-$ZnSnO_3$ structures and their distinguishing features are illustrated in Figure 2. The *il*-$ZnSnO_3$ structure also has Zn and Sn in inequivalent cation positions. The ZnO_6 octahedra have three short oxygen bonds at 2.070 Å and three long bonds at 2.200 Å. The SnO_6 octahedra have 3 short bonds at 2.011 Å and 3 long bonds at 2.160 Å. Distinct cation bonding environments for the $LiNbO_3$ and the ilmenite structure types are expected. Ko and Prewitt[15] discussed how Mn and Ti occupied different positions for the ilmenite versus $LiNbO_3$ ordering in $MnTiO_3$. The different cation positions for each ordering type were attributed to the influence of the edge-sharing

(14) Wells, A. F. *Structural Inorganic Chemistry*, 3rd ed.; Clarendon Press: Oxford, 1962.
(15) Ko, J.; Prewitt, C. T. *Phys. Chem. Miner.* **1988**, *15*, 355–362.
(16) Kovacheva, D.; Petrov, K. *Solid State Ionics* **1998**, *109*, 327–332.
(17) Syono, Y.; Akimoto, S.-I.; Ishikawa, Y.; Endoh, Y. *J. Phys. Chem. Solids* **1969**, *30*, 1665–1672.
(18) Ito, E.; Matsui, Y. *Phys. Chem. Miner.* **1979**, *4*, 265–273.
(19) Abrahams, S. C.; Reddy, J. M.; Bernstein, J. L. *J. Phys. Chem. Solids* **1966**, *27*, 997–1012.
(20) Son, J. Y.; Lee, G.; Jo, M.-H.; Kim, H.; Jang, H. M.; Shin, Y.-H. *J. Am. Chem. Soc.* **2009**, *131*, 8386–8387.

octahedra. $LiNbO_3$ ordering results in Mn−Ti edge-sharing octahedra, whereas ilmenite ordering yields Mn−Mn and Ti−Ti edge-sharing octahedra.

This work reports the *cor*-$In_{2-2x}Zn_xSn_xO_3$ solid solution for $0 \le x \le 0.7$ by high-pressure solid-state synthesis. XRD did not show evidence of long-range ilmenite-type ordering, while a qualitative SHG measurement using 1064 nm radiation[21] revealed a positive response; i.e., green light was observed, indicating $LiNbO_3$-type ordering for $x = 0.6$. The EXAFS of $x = 0.2$ and $x = 0.6$ was consistent with the Zn and Sn octahedra preferentially face-sharing with first-shell oxygen bond lengths similar to those observed for *LN*-$ZnSnO_3$. The best fit to the EXAFS for the range $R = 1-4$ Å for $x = 0.2$ suggested that Zn occupies an off-center position in the octahedron, while Sn resides near the center of the octahedron.

Experimental Section

Synthesis. Stoichiometric amounts of the starting oxides, bixbyite In_2O_3 (Alfa Aesar, 99.99%), rutile SnO_2 (Aldrich, 99.9%), and wurtzite ZnO (Sigma−Aldrich, 99.99%) were ground together in an agate mortar and pestle under acetone and dried under flowing air. Six compositions were chosen that can be described by the general formula $In_{2-2x}Zn_xSn_xO_3$: $x = 0.2$, 0.4, 0.5, 0.6, 0.7, and 0.8. Approximately 0.1 g of powder was loaded into a 12 mm platinum pressure cell (Cyberstar S.A.). The powder mixtures were heated to 1000 °C under 70 kbar pressure. The reaction proceeded at temperature and pressure for 30 min. The temperature was quenched in 2 s followed by a lowering of the pressure at a constant rate. A second reaction procedure for $x = 0.8$ proceeded with a higher temperature of 1150 °C under 70 kbar pressure for a longer time of 60 min.

X-ray Diffraction. Each product was characterized by powder X-ray diffraction (XRD) with a Philips diffractometer using Ni-filtered Cu K_α radiation over the range $2\theta = 5-90°$ and a 0.04° step size and 1 s dwell time. Cell lattice parameters were refined with the program JADE 5.0 (Materials Data Inc.). The XRD pattern of corundum-type In_2O_3 (Cu K_α) was calculated with the program Visualize (version 1.0.1.2) using the crystallographic coordinates determined by Prewitt et al.[11] High-resolution XRD (HR-XRD) patterns of the products for $x = 0.2$ and 0.6 were collected at Argonne National Laboratory Advanced Photon Source facility at Sector 11-BM-B. The samples were mounted in 0.5 mm diameter Kapton capillary tubes and rotated at a speed of 90 revolutions per second during data collection. Discrete detectors covering an angular range from −6 to 16° 2θ are scanned over a 34° 2θ range, with data points collected every 0.001° 2θ and scan speed of 0.01°/s. The data were collected at 100 K using a cryostream LN_2 gas blower (Oxford Cryosystems). The wavelength was calibrated to 0.4122 Å using a mixture of NIST standard reference materials, Si (SRM 640c) and Al_2O_3 (SRM 676).

X-ray Absorption Spectroscopy. The *cor*-ZITO samples ($x = 0.2$ and 0.6) and bixbyite In_2O_3, rutile SnO_2, and wurtzite ZnO standards were prepared for EXAFS measurements by spreading a uniform layer of the powder onto Scotch tape.[22] The standards consisted of 8 layers of tape for transmission mode measurements to obtain $\mu \approx 2$ and $\Delta\mu_0(E) \approx 1$. Because high-pressure reactions yield small amounts of product, the *cor*-ZITO samples were measured in fluorescent mode. A single thin layer of powder was dispersed homogeneously on the tape to minimize self-absorption. The spectra were compared to standard samples measured by transmission mode, such as *bix*-In_2O_3, and significant self-absorption was not observed.

The X-ray absorption spectra were measured at the Argonne National Laboratory Advanced Photon Source (ANL-APS) facility operating at 7.0 GeV with a beam current of 100 mA using the experimental hutch located at Sector 5. Energy selection was performed using a double-crystal monochromator that consisted of two parallel Si(111) crystals, with the second crystal detuned to 70% of the maximum beam intensity in order to reject higher order harmonics. Each measurement included an In, Sn, or Zn metal foil used as a reference to calibrate the absorption edge energy. The edge energy was chosen at the first inflection point—where the second derivative equals zero. The edge energies for the metal reference foils were set to 27 940 eV for In, 29 200 eV for Sn, and 9659 eV for Zn. The standards were measured in transmission mode using Oxford ionization chambers with a path length of 30 cm. The chambers were filled with gas mixtures of He, N_2, and Ar to obtain 10% absorption for the incident beam, I_0, 20% absorption for the sample transmitted beam, I_T, and 60% absorption for the reference foil transmitted beam, I_{T2}. The *cor*-ZITO samples ($x = 0.2$ and 0.6) were measured in fluorescent mode with a 13-element Ge solid-state detector. The detector was placed at a 90° angle with respect to the beam path. Each measurement consisted of six replicates to improve the data quality with an increased signal-to-noise ratio.

Background removal was performed using the AutoBK algorithm[23,24] as implemented in Athena,[25] a graphical front-end for the IFFEFIT[25−27] software package. The data were normalized to an edge step height of one. Approximately halfway up the absorption edge defined the edge energy, E_0, which was used to determine the photoelectron wavenumber: $k = (2m_e(E - E_0)/\hbar^2)^{1/2}$, where m_e is the electron mass, $\hbar$ is Planck's constant, and E is the incident X-ray energy. For the In and Sn K edge, the samples and standards were measured from 250 eV below the edge to 1230 eV above the edge ($k = 18$ Å^{-1}). For the Zn K edge, the samples and standards were measured from 150 eV below the edge to 1230 eV above the edge. The $\chi(k)$ spectra were Fourier transformed with a sine window over the region $k = 2.4-10.0$ Å^{-1} for the In data, $k = 2.35-10.7$ Å^{-1} for the Sn data, and $k = 2.4-9.8$ Å^{-1} for the Zn data, which yields a complex function with a real and imaginary component. Modeling and simulations of the EXAFS spectra were performed using the FEFF 6.0 code[28] as implemented in Artemis.[25] The goodness-of-fit was determined by minimizing the residual component, $R = \sum_i(\text{data}_i - \text{fit}_i)^2/\sum_i\text{data}_i^2$, between the model and experimental values of the k^2-weighted data.[29] All the Fourier transforms shown are uncorrected for phase shifts.

Second Harmonic Generation. Powder SHG measurements were performed on a modified Kurtz-NLO system[30] using a pulsed Nd:YAG laser with a wavelength of 1064 nm. A detailed description of the equipment and methodology has been published.[21]

Results and Discussion

The products of the high-pressure reaction for the compositions $x = 0.2-0.7$ exhibited XRD patterns with peaks characteristic of a corundum-type structure as the major phase, trace amounts of SnO_2, and an unknown phase (Figure 3). The unknown phase could not be identified as any known phase in the $ZnO-In_2O_3-SnO_2$ bulk equilibrium or residual Pt from the

(21) Ok, K. M.; Chi, E. O.; Halasyamani, P. S. *Chem. Soc. Rev.* **2006**, *35*, 710–717.
(22) Mason, T. O.; Gonzalez, G. B.; Hwang, J.-H.; Kammler, D. R. *Phys. Chem. Chem. Phys.* **2003**, *5*, 2183–2189.
(23) Newville, M.; Livins, P.; Yacoby, Y.; Rehr, J. J.; Stern, E. A. *Jpn. J. Appl. Phys. Part I* **1993**, *32* (Supplement), 125–127.
(24) Ravel, B.; Newville, M.; Cross, J. O.; Bouldin, C. E. *Physica B* **1995**, *209*, 145–147.
(25) Ravel, B.; Newville, M. *J. Synchrotron Radiat.* **2005**, *12*, 537–541.
(26) Newville, M. *J. Synchrotron Radiat.* **2001**, *8*, 96–100.
(27) Newville, M. *J. Synchrotron Radiat.* **2001**, *8*, 322–324.
(28) Rehr, J. J.; Zabinsk, S. I. FEFF5: An ab Initio Multiple Scattering XAFS Code, Department of Physics, University of Washington, 1992.
(29) Kelly, S. D.; Hesterberg, D.; Ravel, B. In *Methods of Soil Analysis. Part 5. Mineralogical Methods*; Ulery, A. L., Drees, L. R., Eds.; Soil Society of America, Inc.: Madison, WI, 2008; Vol. 5.
(30) Kurtz, S. K.; Perry, T. T. *J. Appl. Phys.* **1968**, *39*, 3798.

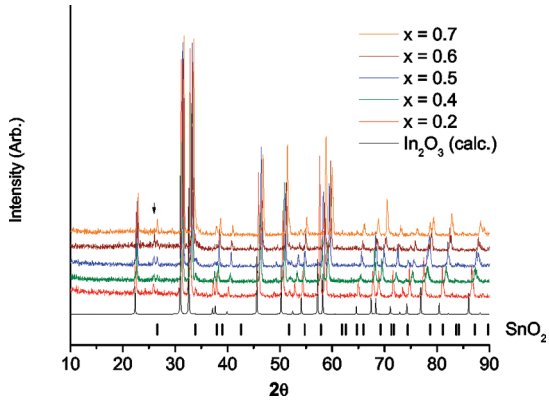

Figure 3. XRD patterns of high-pressure products for $x = 0.2-0.7$ and the calculated XRD pattern of corundum In_2O_3 (no $K_{\alpha 2}$). The peak positions for SnO_2 (PDF #41−1445) are marked below the XRD patterns. The peak at $2\theta \sim 25°$ corresponding to the unknown phase is indicated with an arrow.

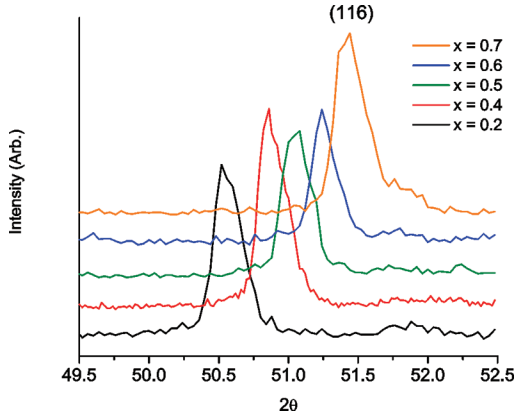

Figure 4. XRD of the *cor*-ZITO (116) reflection demonstrating how the peak positions shift to higher angles with increased Zn and Sn substitution (higher x).

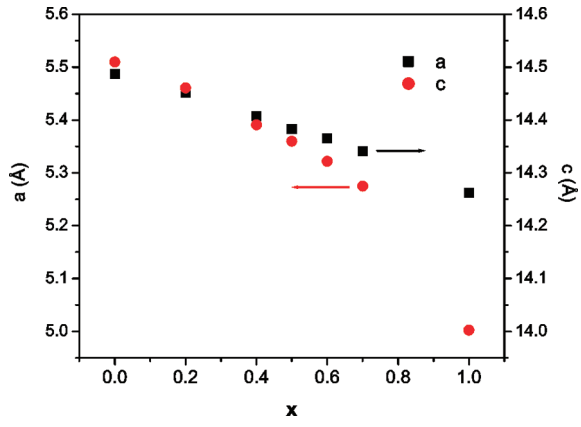

Figure 5. Plot of unit cell a (black box) and c (red circle) lattice constants as a function of x. The reported end members, *cor*-In_2O_3[11] ($x = 0$) and *LN*-$ZnSnO_3$[13] ($x = 1$) are also included.

reaction crucible. The unknown was observed as a trace secondary phase for the high-pressure synthesis of *LN*-$ZnSnO_3$.[13] The XRD reflections of *cor*-ZITO shift to higher angles at larger values of x indicative of a lattice contraction (Figure 4). The lattice parameters for the products at $x = 0.2-0.7$, *cor*-In_2O_3,[11] and *LN*-$ZnSnO_3$[13] are plotted in Figure 5 and listed in Table 1. The a-axis decreases in a linear manner, while the c-axis decreases in a nonlinear fashion. The c/a ratio for the solid solution stays within the range 2.64−2.67. The lattice contraction is consistent with the cosubstitution of In^{3+} (0.80 Å) by the smaller Zn^{2+} (0.74 Å) and Sn^{4+} (0.69 Å) cations.[31] The XRD patterns do not exhibit the (003) or (101) ilmenite reflections at $2\theta \sim 18.4°$ and $\sim 19.9°$, respectively. The cations, however, may exhibit partial ordering, which would cause the ilmenite reflections to be weak. HR-XRD patterns of *cor*-ZITO for $x = 0.2$ and 0.6 were examined to identify potential partial ordering. Figure 6 shows the full HR-XRD pattern with the low angles expanded in the inset. The (003) and (101) ilmenite reflections were not observed above the noise level.

Table 1. Cell Constants for *cor*-$In_{2-2x}Zn_xSn_xO_3$ ($x = 0.2-0.7$), *cor*-In_2O_3, and *LN*-$ZnSnO_3$

$In_{2-2x}Zn_xSn_xO_3$, x	a (Å)	c (Å)	cell volume (Å^3)	c/a
0 (*cor*-In_2O_3)[11]	5.487	14.510	378.33	2.64
0.2	5.451(16)	14.461(1)	372.19	2.65
0.4	5.407(2)	14.391(3)	364.41	2.66
0.5	5.383(1)	14.360(3)	360.49	2.67
0.6	5.365(2)	14.322(5)	357.05	2.67
0.7	5.341(1)	14.275(2)	352.62	2.67
1.0 (*LN*-$ZnSnO_3$)[13]	5.262	14.003	335.79	2.66

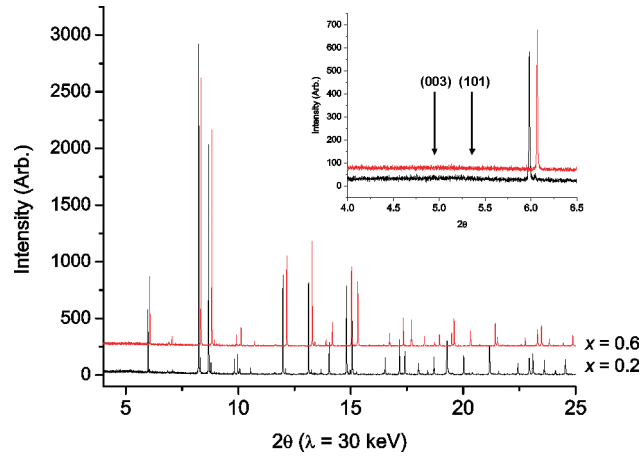

Figure 6. High-resolution XRD patterns of *cor*-$In_{2-2x}Zn_xSn_xO_3$ for $x = 0.2$ (bottom, black) and $x = 0.6$ (top, red). The inset is the low-angle region expanded with the approximate location of where the (003) and (101) ilmenite-type reflections would appear indicated by the arrows.

Because $LiNbO_3$-type ordering exhibits the same reflections as corundum-type ordering, the diffraction patterns will differ only in their relative peak intensities. The simulated diffraction patterns for $x = 0.6$ show a small difference in relative intensities, I_{rel}, of 24.78 and 19.13, respectively, for the (012) reflection when the (104) was normalized to $I_{rel} = 100$. The experimental high-resolution XRD pattern of *cor*-ZITO for $x = 0.6$ showed $I_{rel} = 23.12$ for the (012) reflection, which suggests *cor*-ZITO exhibits $LiNbO_3$-type ordering (see Supporting Information for Tables S1, S2, and S3 and Figure S1). The relative intensities of the remaining diffraction peaks for $R3c$ and $R\bar{3}c$ are very similar. If Zn and Sn exhibit some degree of polar order ($R3c$ space group), then the powder should generate a second harmonic response. The *cor*-ZITO solid solution sample prepared for $x = 0.6$ was irradiated with a 1064 nm laser beam and 532 nm green light was observed, which indicated $LiNbO_3$-type ordering at some length scale (∼micrometer lengths). Inaguma et al.[13] found that the synthesis under high pressure of $ZnSnO_3$ with a $LiNbO_3$-type structure results in a polar material, i.e., a crystal structure where Zn and Sn are ordered.

(31) Shannon, R. D. *Acta. Crystallogr., Sect. A* **1976**, *32*, 751–767.

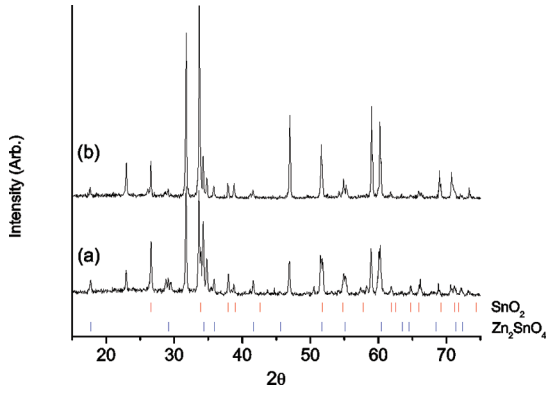

Figure 7. XRD of products obtained from high-pressure reactions at $x = 0.8$. The two reaction conditions were (a) 1000 °C, 70 kbar for 30 min and (b) 1150 °C, 70 kbar for 60 min. The PDF lines for the secondary phases SnO_2 (top, red, #41−1445) and Zn_2SnO_4 (bottom, blue, #24−1470) are shown.

The product of the reaction for $x = 0.8$ at 1000 °C and 70 kbar for 30 min was a mixture of *cor*-ZITO, SnO_2, and $Zn_{1.89}Sn_{0.89}In_{0.22}O_4$ (In-substituted Zn_2SnO_4 spinel[32]). The lattice parameters for *cor*-ZITO were $a = 5.332(1)$ Å and $c = 14.237(6)$ Å, which extrapolate to the approximate composition $In_{0.56}Zn_{0.72}Sn_{0.72}O_3$ ($x = 0.72$) based on the a cell constant. The reaction for $x = 0.8$ was repeated at 1150 °C under 70 kbar for 60 min. The secondary phases $Zn_{1.89}Sn_{0.89}In_{0.22}O_4$ (spinel) and SnO_2 were present, but in lower amounts as shown in Figure 7. The lattice parameters of the *cor*-ZITO phase changed to $a = 5.322(1)$ Å and $c = 14.245(4)$ Å, which corresponds to the approximate composition $In_{0.48}Zn_{0.76}Sn_{0.76}O_3$ ($x = 0.76$). Although the fully substituted corundum-type structure was not observed for $x = 0.8$, the increased cosubstitution with increased reaction time and temperature suggests that *cor*-$In_{0.4}Zn_{0.8}Sn_{0.8}O_3$ ($x = 0.8$) is the stable thermodynamic product. Formation of In-substituted Zn_2SnO_4 and SnO_2 may fall into a local energy minimum and increase the reaction time. A similar problem was encountered during the formation of the $(ZnO)_kIn_2O_3-SnO_2$ equilibrium products in the $ZnO-In_2O_3-SnO_2$ subsolidus system at ambient pressure.[9] The thermodynamic products would not form when ZnO, In_2O_3, and SnO_2 were used as the starting reagents owing to slow kinetics. The use of different starting reagents, such as $Zn_{11}In_2O_{14}$ and In-substituted Zn_2SnO_4, led to the formation of the thermodynamic products.[9] Therefore, the reaction to form *cor*-$In_{0.4}Zn_{0.8}Sn_{0.8}O_3$ could be approached by starting with *cor*-In_2O_3 and *LN*-$ZnSnO_3$ rather than bixbyite In_2O_3, SnO_2, and ZnO. The *LN*-$ZnSnO_3$ end member is favored over Zn_2SnO_4 and SnO_2 at 70 kbar and 1000 °C, which supports *cor*-$In_{0.4}Zn_{0.8}Sn_{0.8}O_3$ as the thermodynamic product. The *cor*-$In_{2-2x}Zn_xSn_xO_3$ solid solution for $0.7 < x < 1.0$ may exist, but it remains unverified.

Extended X-ray Absorption Fine Structure. The Zn and Sn local coordination environment in the *cor*-ZITO solid solution was investigated by EXAFS. The first coordination shell for In, Sn, and Zn within *cor*-ZITO for $x = 0.2$ and 0.6 will be discussed. Then, the proposed local structures of In, Sn, and Zn within a 4 Å range ($R = 1-4$ Å) for $x = 0.2$ will be discussed. The passive electron reduction factors for In, Sn, and Zn were determined to be 1.0 from the In_2O_3, SnO_2, and ZnO standards. The details of these fits are presented by Hoel et al.[33] Owing to thermal vibrations and the relative displacements of an atom from its ideal position, each neighbor is modeled with a Gaussian distribution factor, $e^{-2\sigma^2k^2}$, where the variance, σ^2, is referred to as the mean square relative displacement (MSRD). The measurements presented throughout this paper were all taken at room temperature, so the MSRD cannot be separated from the thermal vibration term, σ^2_{th}, and positional displacement term, σ^2_{displ}. Because the measurements were taken at the same temperature, the thermal vibration term will not vary between individual samples. The degree of the relative displacement of the neighbor position will dominate variations of σ^2.

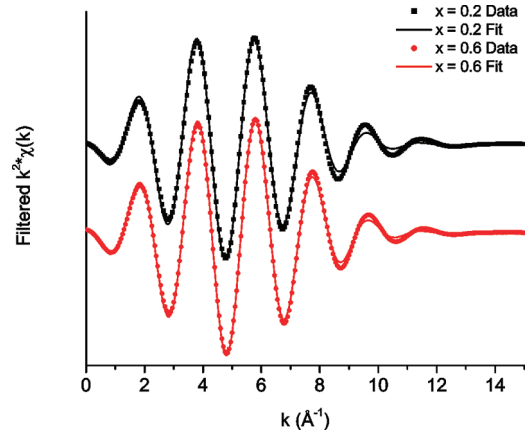

Figure 8. Best fit of *cor*-ZITO for $x = 0.2$ (top, black line) and $x = 0.6$ (bottom, red line) overlaying the experimental spectrum ($x = 0.2$, black squares; $x = 0.6$, red circles) at the In K edge plotted as the real component of the filtered first shell.

Table 2. Values for the Best Fits to the First Shell of the *cor*-ZITO Spectra at $x = 0.2$ and 0.6 at the In K Edge[a]

cor-ZITO	*R*(3 In−O) (Å)	*R*(3 In−O) (Å)	σ^2 (Å^2)	ΔE_0 (eV)	*R*-factor
$x = 0$	2.12	2.26			
$x = 0.2$	2.08(2)	2.23(2)	0.0049(13)	1.1(1.6)	0.016
$x = 0.6$	2.07(1)	2.22(1)	0.0035(8)	1.6(1.1)	0.006

[a] The listed bond lengths for $x = 0$ are the crystallographic values for *cor*-In_2O_3 from Prewitt et al.[11]

Table 3. Values for the Best Fits to the First Shell of the *cor*-ZITO Spectra at $x = 0.2$ and 0.6 at the Sn K Edge[a]

cor-ZITO	*R*(6 Sn−O) (Å)	σ^2 (Å^2)	ΔE_0 (eV)	*R*-factor
$x = 0.2$	2.080(7)	0.0038(8)	2.8(8)	0.007
$x = 0.6$	2.073(7)	0.0049(6)	2.8(8)	0.007
$x = 1.0$	2.005/2.094			

[a] The bond lengths for $x = 1.0$ are the crystallographic values for *LN*-$ZnSnO_3$ from Inaguma et al.[13]

First Shell of *cor*-ZITO for $x = 0.2$ and 0.6—In, Sn, and Zn Edges. The first coordination shells of In, Sn, and Zn in *cor*-ZITO at $x = 0.2$ and 0.6 were fit over the range $R = 1-2.2$ Å. The real component of the Fourier filtered $k^2 \cdot \chi(k)$ and best first-shell fits of *cor*-ZITO at the In edge are plotted in Figure 8. The best fit results for the first shell of the EXAFS for In, Sn, and Zn are listed in Tables 2, 3, and 4, respectively. The first In−O shell was fit with 3 short O bonds at ~2.08 Å and 3 long O bonds at ~2.23 Å. The first Sn−O shell was fit with 6 O at a single bond length of ~2.08 Å. The first Zn−O shell was fit with 3 short O bonds at ~2.02 Å and 3 long O bonds at ~2.38 Å with separate MSRDs for each bond length.

(32) Palmer, G. B.; Poeppelmeier, K. R.; Mason, T. O. *J. Solid State Chem.* **1997**, *134*, 192–197.

(33) Hoel, C. A.; Gaillard, J.-F.; Poeppelmeier, K. R. *J. Solid State Chem.* **2010**, *183*, 761–768.

Table 4. Values for the Best Fits to the First Shell of the *cor*-ZITO Spectra at $x = 0.2$ and 0.6 at the Zn K Edge[a]

cor-ZITO	*R*(3 Zn−O1) (Å)	*R*(3 Zn−O2) (Å)	σ^2_{O1} (Å^2)	σ^2_{O2} (Å^2)	ΔE_0 (eV)	*R*-factor
$x = 0.2$	2.03(1)	2.37(3)	0.0089(8)	0.028(5)	2.5(1.3)	0.010
$x = 0.6$	2.01(1)	2.39(3)	0.0089(8)	0.028(5)	2.5(1.3)	0.005
$x = 1.0$	2.041	2.310				

[a] The MSRDs, σ^2_{O1} and σ^2_{O2}, and energy shift, ΔE_0, were refined to the same values for $x = 0.2$ and 0.6. The bond lengths for $x = 1.0$ are the crystallographic values for *LN*-$ZnSnO_3$ from Inaguma et al.[13]

The first-shell In−O distances are similar for *cor*-ZITO at $x = 0.2$ and 0.6, which indicates the In local bonding environment is not strongly influenced by Zn and Sn substitution. This result is consistent with InO_6 octahedra preferentially face-sharing InO_6 octahedra rather than SnO_6 or ZnO_6 octahedra. The position of the In cation, which is inferred from the In−O bond lengths, is sensitive to the charge and proximity of the cation in the face-sharing octahedron. The Sn−O bond lengths are similar for *cor*-ZITO at $x = 0.2$ and 0.6, and the Zn−O bond lengths are similar for $x = 0.2$ and 0.6. Therefore, the Sn and Zn local bonding environments are not influenced strongly by the degree of substitution, consistent with Zn and Sn octahedra preferentially face-sharing with each other. It is notable that the InO_6, SnO_6, and ZnO_6 octahedra each have very different metal−oxygen bond lengths and are insensitive to the composition (value of *x*). The bond lengths of substitutional cations have been predicted and experimentally observed to relax to bond lengths that are close to the end members owing to the "constancy of the ionic radii".[31,34−36] For *cor*-$In_{2-2x}Zn_xSn_xO_3$, the Zn and Sn local coordination environments relax to form Zn−O and Sn−O bond lengths that are similar to those observed for *LN*-$ZnSnO_3$, which corresponds to $x = 1.0$ by this high-pressure/high-temperature synthesis route. Furthermore, the In−O bond lengths are similar to those in unsubstituted *cor*-In_2O_3 ($x = 0$). Structural relaxation was also observed for bixbyite ZITO such that the Zn−O and Sn−O bond lengths were short owing to the small cationic radii and the In−O bond length was similar to unsubstituted In_2O_3.[33]

The first oxygen shell of Sn does not exhibit the asymmetric coordination environment characteristic of the corundum structure. Instead, the Sn cation forms 6 equal bonds to O at 2.08 Å such that the bonding environment is more similar to that of *LN*-$ZnSnO_3$ (3 O at 2.00 Å and 3 O at 2.09 Å) than that of *cor*-In_2O_3 (3 O at 2.08 Å and 3 O at 2.23 Å). The Sn−O bond lengths in *cor*-ZITO can be explained by examination of the bond valence sum (BVS) for the Sn^{4+} cation. If the Sn local environment was the same as In with 3 O bonded at 2.08 Å and 3 O bonded at 2.23 Å, then $BVS_{Sn} = 3.12$ ($R_0 = 1.905$, $B = 0.37$).[37−40] When the local Sn environment adopts 6 O bonded at 2.08 Å, then $BVS_{Sn} = 3.76$, which is more favorable. The first oxygen shell for Zn exhibits a large difference in bond lengths of 2.03 and 2.37 Å, which is similar to that in *LN*-$ZnSnO_3$ (2.04 and 2.31 Å). If Zn ($R_0 = 1.704$, $B = 0.37$) adopted the corundum first-shell coordination of 3 O at 2.08 Å and 3 O at 2.23 Å, then $BVS_{Zn} = 1.82$. Zn in *cor*-ZITO, however, has 3 O at 2.03 Å and 3 O at 2.37 Å so that $BVS_{Zn} = 1.74$. The different Zn environment is due to the presence of the large positive charge of the face-sharing Sn^{4+} cation repulsing Zn further from the face-sharing oxygen. The first-shell coordination environments, thus, support the formation of In−In and Zn−Sn face-sharing octahedra over possible In−Zn, In−Sn, and very unlikely Zn−Zn and Sn−Sn combinations.

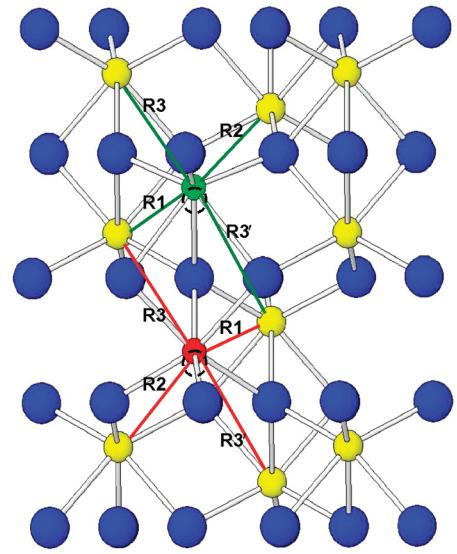

Figure 9. Depiction of how the neighbor distances change when Zn (top, green) and Sn (bottom, red) shift away from the In (yellow) position. The dashed black circles represent the corundum cation position, and the blue spheres are oxygen. *R*1 represents the new distance to the 3 In previously at 3.243 Å, and *R*2 represents the new distance to the 3 In previously at 3.606 Å. *R*3 represents the new shorter distance to 3 of the 6 In previously at 3.986 Å. *R*3′ represents the new longer distance to the remainder 3 of the In.

EXAFS of *cor*-ZITO for $x = 0.2$—In, Sn, and Zn Edges. The first-shell bond lengths suggest that Sn resides close to the center of the octahedron and Zn is far away from the center. If Zn and Sn occupy positions in the oxygen octahedra that are different from the In position, then the cation neighbor distances will be different. This effect is illustrated in Figure 9. The *cor*-In_2O_3 local structure consists of one In neighbor at 3.114 Å (second shell), three In at 3.243 Å (third shell), three In at 3.606 Å (fourth shell), six In at 3.986 Å (fifth shell), and one In at 4.141 Å (sixth shell). If Zn is displaced further from the octahedral center, compared to In in *cor*-In_2O_3, then the third shell In will be further (*R*1), the fourth shell In will be closer (*R*2), and the fifth shell will split into two separate distances of three closer In (*R*3) and three further In (*R*3′). If Sn occupies the center of the octahedron, the In neighbor distances will exhibit the opposite effect as the Zn neighbor distances.

The proposed structure was fit to the EXAFS of the In, Sn, and Zn K edges for the range $R = 1-4.0$ Å. The *cor*-ZITO $k^2 \cdot \chi(k)$ and real component of the Fourier transform for the experimental data and fit of the In, Sn, and Zn K edges are plotted in Figures 10, 11, and 12 with the best fit values listed in Tables 5, 6, and 7, respectively. The *cor*-In_2O_3 single-crystal neighbor distances and coordination numbers are listed for comparison. Owing to the large number of shells, Zn and Sn octahedral positions, and three cation types, two assumptions were used to reduce the number of correlated variables. First, the face-sharing octahedral units were either pairs of In−In or

(34) Zunger, A.; Jaffe, J. E. *Phys. Rev. Lett.* **1983**, *51*, 662–665.
(35) Martins, J. L.; Zunger, A. *Phys. Rev. B* **1984**, *30*, 6217–6220.
(36) Nakagawa, T.; Osuki, T.; Yamamoto, T. A.; Kitauji, Y.; Kano, M.; Katsura, M.; Emura, S. *J. Synchrotron Rad.* **2001**, *8*, 740–742.
(37) Brown, I. D.; Shannon, R. D. *Acta Crystallogr., Sect. A* **1973**, *29*, 266–282.
(38) Altermatt, D.; Brown, I. D. *Acta Crystallogr., Sect. B* **1985**, *41*, 240–244.
(39) Brown, I. D.; Altermatt, D. *Acta Crystallogr., Sect. B* **1985**, *41*, 244–247.
(40) Brese, N. E.; O'Keeffe, M. *Acta Crystallogr., Sect. B* **1985**, *47*, 192.

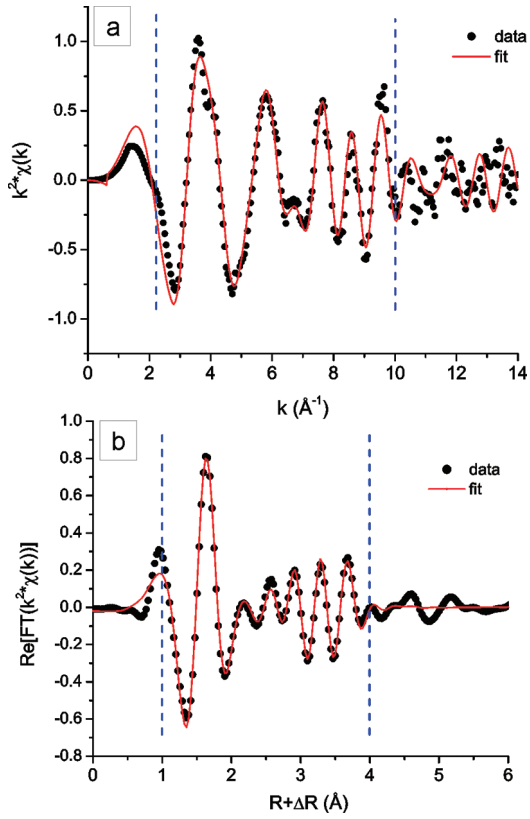

Figure 10. Best fit of *cor*-ZITO for $x = 0.2$ (red line) overlaying the experimental spectrum (black dots) at the In K edge plotted as $k^2 \cdot \chi(k)$ (top) and the real component of the k^2-weighted Fourier transform (bottom). The Fourier transform window, $k = 2.4-10.0$ Å^{-1}, and fitting range, $R = 1-4.0$ Å, are marked with the vertical blue dashed lines. R-factor = 0.011.

Table 5. Values for the Best Fit to the *cor*-ZITO Spectrum at $x = 0.2$ at the In K Edge[a]

neighbor	crystal C.N. *cor*-In_2O_3	crystal *R* (Å) *cor*-In_2O_3	EXAFS C.N. *cor*-ZITO	EXAFS *R* (Å) *cor*-ZITO
O (O1)	3	2.117	3	2.08(1)
O (O2)	3	2.258	3	2.23(1)
In	1	3.114	1	3.13(5)
In	3	3.243	2.4	3.25(2)
Sn			0.3	3.24(3)
Zn			0.3	3.20(3)
In	3	3.606	2.4	3.55(4)
Sn			0.3	3.64(5)
Zn			0.3	3.48(1)
O	3	3.668	3	3.62(1)
In (In4)	6	3.986	4.8	3.96(2)
Sn			0.3	3.85(3)
Sn			0.3	4.07(3)
Zn			0.3	3.87(1)
Zn			0.3	4.07(1)
In	1	4.141	1	4.10(5)
O	3	4.421	3	4.38(1)
In4 − O1 (MS)			4.8	4.15(2)
In4 − O2 (MS)			4.8	4.15(2)

[a] Note: $S_0^2 = 1.0$, $\Delta E_0 = 1.5$ eV, $\sigma^2_{O1} = \sigma^2_{O2} = 0.005(1)$ Å^2; $\sigma^2 = 0.006(2)$ Å^2 for all other scattering paths.

Zn−Sn. Face-sharing In−Sn, In−Zn, Sn−Sn, and Zn−Zn octahedra were excluded from the fit. The second assumption was that Sn and Zn did not form clusters, that is, the composition of the cation neighbors for the In edge was 8:1:1 for In:Sn:Zn, and that Zn and Sn had only In cation neighbors with the exception of the face-sharing octahedron. The models for the In, Sn, and Zn edge data sets were fit for a single refinement

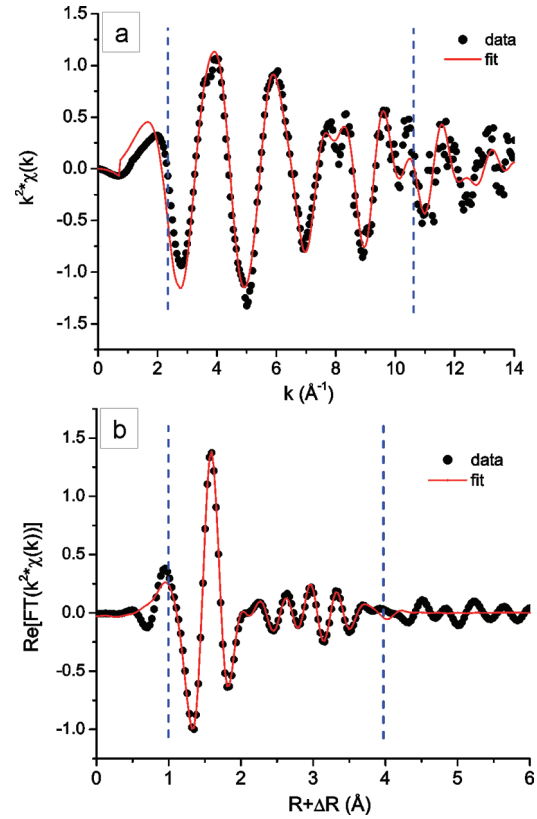

Figure 11. Best fit of *cor*-ZITO for $x = 0.2$ (red line) overlaying the experimental spectrum (black dots) at the Sn K edge plotted as $k^2 \cdot \chi(k)$ (top) and the real component of the k^2-weighted Fourier transform (bottom). The Fourier transform window, $k = 2.35-10.7$ Å^{-1}, and fitting range, $R = 1-4.0$ Å, are marked with the vertical blue dashed lines. R-factor = 0.005.

Table 6. Values for the Best Fit to the *cor*-ZITO Spectrum at $x = 0.2$ at the Sn K Edge[a]

neighbor	crystal C.N. *cor*-In_2O_3	crystal *R* (Å) *cor*-In_2O_3	EXAFS C.N. *cor*-ZITO	EXAFS *R* (Å) *cor*-ZITO
O (O1)	3/3	2.117/2.258	6	2.079(5)
Zn	1	3.114 (In)	1	3.20(8)
In	3	3.243	3	3.24(3)
In	3	3.606	3	3.64(4)
In	3	3.986	3	3.85(3)
In	3	3.986	3	4.07(3)
In	1	4.141	1	4.227
O	3	4.155	3	4.13(8)
O	3	4.421	3	4.13(8)

[a] Note: $S_0^2 = 1.0$, $\Delta E_0 = 2.0$ eV, $\sigma^2_{O1} = 0.004(1)$ Å^2; $\sigma^2 = 0.007(3)$ Å^2 for all other scattering paths.

(i.e., multiedge refinement) to ensure consistent neighbor distances between each local structure model.

The In edge first-shell was fit with 3 O neighbors at 2.08 Å and 3 O at 2.23 Å. As mentioned in the previous section, these In−O bond distances are similar to those in *cor*-In_2O_3. The second-shell nearest cation neighbor distance to the In face-sharing octahedron was determined to be at 3.13 Å. The third shell of neighbors was fit by 3 cations with fractional occupancies of 0.8 for In, 0.1 for Sn, and 0.1 for Zn. The neighbor distances (*R*1) were 3.25 Å for In, 3.24 Å for Sn, and 3.20 Å for Zn. Despite the different octahedral cation positions of Zn and Sn, the neighbor distances are similar to those of corundum In_2O_3, possibly due to the additional effect of the first-shell oxygen bond relaxation. The fourth shell was fit with 3 cation neighbors with fractional occupancies of 0.8 for In, 0.1 for Sn,

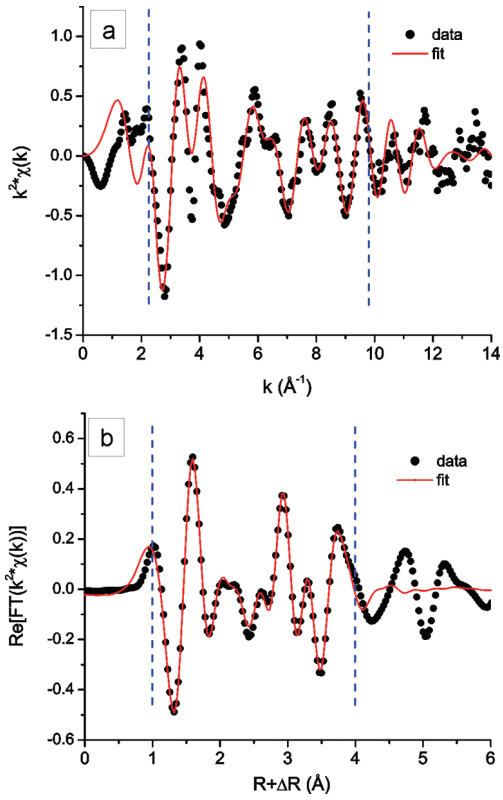

Figure 12. Best fit of *cor*-ZITO for $x = 0.2$ (red line) overlaying the experimental spectrum (black dots) at the Zn K edge plotted as $k^2 \cdot \chi(k)$ (top) and the real component of the k^2-weighted Fourier transform (bottom). The Fourier transform range, $k = 2.4-9.8$ Å^{-1}, and fitting range, $R = 1-4.0$ Å, are marked with the vertical blue dashed lines. R-factor = 0.010.

Table 7. Values for the Best Fit to the *cor*-ZITO Spectrum at $x = 0.2$ at the Zn K Edge[a]

neighbor	crystal C.N. *cor*-In_2O_3	crystal *R* (Å) *cor*-In_2O_3	EXAFS C.N. *cor*-ZITO	EXAFS *R* (Å) *cor*-ZITO
O (O1)	3	2.117	3	2.021(6)
O (O2)	3	2.258	3	2.36(2)
Sn	1	3.114	1	3.20(8)
In	3	3.243	3	3.20(3)
In (In3)	3	3.606	3	3.48(2)
O	3	3.668	3	3.66(4)
O	3	3.807	3	3.69(6)
In (In4s)	3	3.986	3	3.87(1)
In (In4l)	3	3.986	3	4.06(1)
O	3	4.155	3	4.02(6)
In	1	4.141	1	4.027
O	3	4.735	3	4.82(6)
In3 − O1 (MS)			6	3.80(1)
In4s − O1 (MS)			3	4.07(1)
In4l − O1 (MS)			3	4.16(1)

[a] Note: $S_0^2 = 1.0$, $\Delta E_0 = 0$ eV, $\sigma^2_{O1} = 0.009(1)$ Å^2, $\sigma^2_{O2} = 0.024(4)$ Å^2; $\sigma^2 = 0.010(1)$ Å^2 for all other scattering paths.

and 0.1 for Zn. A minor contraction is observed for the In neighbor at 3.55 Å compared to *cor*-In_2O_3 at 3.61 Å, as expected from the lattice contraction. The Sn neighbor is at a longer distance of 3.64 Å ($R2_{Sn}$), and the Zn neighbor is at a shorter distance of 3.48 Å ($R2_{Zn}$), predicted from the Zn and Sn positions in the octahedra. The fifth shell of cation neighbors included six cations with fractional occupancies of 0.8 for In, 0.1 for Sn, and 0.1 for Zn. The In neighbors were fit with a single distance of 3.96 Å, which is slightly shorter than the *cor*-In_2O_3 distance of 3.99 Å. The Sn and Zn neighbors were fit so that half of the Sn were at 3.85 Å ($R3_{Sn}$) and half were at 4.07 Å ($R3_{Sn}'$), while half the Zn neighbors were at 3.87 Å ($R3_{Zn}$) and half were at 4.06 Å ($R3_{Zn}'$). The splitting of the In−Zn and In−Sn neighbors for the fifth shell is consistent with Sn nearby the octahedral center and Zn occupying a position far from the octahedral center. The sixth cation shell was fit as 1 In at 4.10 Å, which is similar to the corundum In_2O_3 structure. Additional contributions from O shells and multiple scattering from O and In neighbors that were included in the fit are listed in Tables 5, 6, and 7. From the first coordination shells and the multiple-shell fit, it is apparent that the ZnO_6 and SnO_6 octahedra in *cor*-ZITO are similar to the octahedra in *LN*-$ZnSnO_3$. The EXAFS, however, cannot be used to suggest local $LiNbO_3$-type ordering of the Zn−Sn dipole because it was fit as an isolated unit in the host *cor*-In_2O_3. Fits of the EXAFS of the Sn and Zn edges were attempted that assumed Zn and Sn occupied the same octahedral positions as In in *cor*-ZITO, but a reasonable fit could not be obtained.

The multiedge refinement of the In, Sn, and Zn EXAFS decreased the total number of variables, which lowered the uncertainties that were obtained for the neighbor distances and improved the confidence of the proposed structure. There were a few shell distances, however, that had large uncertainties, such as the Sn−Zn (or Zn−Sn) octahedral face-sharing neighbor at 3.20 Å. Owing to the weak contribution of one cation neighbor in the shell, the fit is not sensitive to this distance, so a large uncertainty of 0.08 Å is observed. The distance of the face-sharing In−In cations is within uncertainty of the distance of the Zn−Sn face-sharing cations as expected from the cation positions in the octahedra.

Conclusion

The corundum-type solid solution $In_{2-2x}Zn_xSn_xO_3$ ($0 \le x \le 0.7$) formed at elevated pressures of 70 kbar and temperatures over 1000 °C. Utilization of XRD and EXAFS elucidated a detailed description of the substitution of Zn and Sn for In in corundum-In_2O_3. The Zn and Sn substituents form face-sharing octahedra with each other. The Zn and Sn local environments relax such that the Zn−O and Sn−O first-shell bond lengths are similar to those observed in *LN*-$ZnSnO_3$ rather than *cor*-In_2O_3. In addition, Zn is displaced far from the octahedral center, while Sn occupies a position closer to the octahedral center. Ilmenite-type long-range cation ordering was not detected by HR-XRD, while a $LiNbO_3$-type arrangement for $x = 0.6$ was shown by observation of an SHG response using 1064 nm radiation. The experimental results of the local coordination environment of In, Sn, and Zn, in general, can be extended to further understand complex structures and systems, such as amorphous TCOs.

Acknowledgment. C.A.H. was funded through the Materials Research Science and Engineering Center at Northwestern University supported by the National Science Foundation under NSF Award Number DMR-0520513. The work was performed at the DuPont−Northwestern−Dow Collaborative Access Team (DND-CAT) located at Sector 5 of the Advanced Photon Source (APS). DND-CAT is supported by E. I. Dupont de Nemours & Co., The Dow Chemical Company, and the State of Illinois. Use of the APS was supported by the U.S. Department of Energy, Office of Science, Office of Basic Energy Sciences, under Contract No. DE-AC02-06CH11357. The authors thank Dr. Qing Ma for assistance with the EXAFS measurements and helpful discussions and the 11-BM staff for assistance with the HR-XRD measurements. C.A.H. and K.R.P. thank T. O. Mason for helpful discussions. We also thank

CICYT (Spain) through project MAT2004-01641 and MAT2007-64006, as well as Comunidad Autonome de Madrid through the MATERYENER program PRICYT S-0505/PPQ-0093 (2006). We thank the reviewer for suggesting the qualitative SHG test to detect the $LiNbO_3$-type ordering and Jeongho Yeon and P. Shiv Halasyamani (University of Houston) for the SHG measurements.

Supporting Information Available: Comparison of the expected X-ray diffraction patterns of *cor*-$In_{0.8}Zn_{0.6}Sn_{0.6}O_3$ ($x = 0.6$) based on the $R3c$ and $R\bar{3}c$ space groups. This material is available free of charge via the Internet at http://pubs.acs.org.

JA106048X